Lawrence Berkeley National Laboratory
Recent Work

Title
Graphene Membranes for Atmospheric Pressure Photoelectron Spectroscopy.

Permalink
https://escholarship.org/uc/item/6401c0rt

Journal
The journal of physical chemistry letters, 7(9)

ISSN
1948-7185

Authors

Weatherup, Robert S
Eren, Baran
Hao, Yibo
et al.

Publication Date
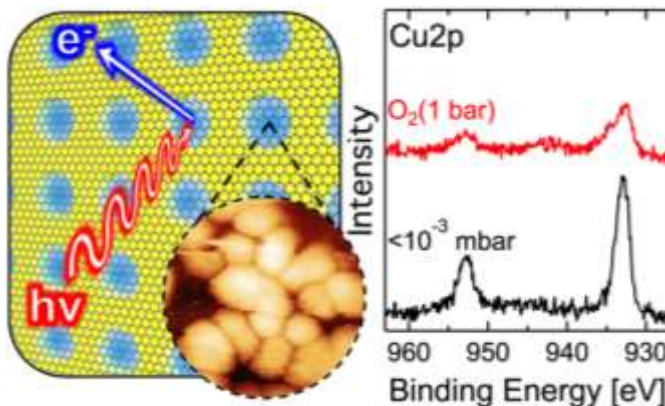2016-05-01

DOI
10.1021/acs.jpclett.6b00640

Peer reviewed

Graphene Membranes for Atmospheric Pressure Photoelectron Spectroscopy

Robert S. Weatherup[1], Baran Eren[1], Yibo Hao[1], Hendrik Bluhm[2] and Miquel B. Salmeron[1,3,*]

1Materials Sciences Division and 2Chemical Sciences Division, Lawrence Berkeley National Laboratory, 1 Cyclotron Road, Berkeley, California 94720, United States

3Department of Materials Science and Engineering, University of California, Berkeley, California 94720-1760, United States

ABSTRACT: Atmospheric pressure x-ray photoelectron spectroscopy (XPS) is demonstrated using atomically-clean single-layer graphene membranes as photoelectron-transparent barriers that sustain pressure differences in excess of 6 orders of magnitude. The graphene serves as a support for catalyst nanoparticles under atmospheric pressure reaction conditions (up to 1.5 bar), where XPS allows the oxidation state of Cu nanoparticles and gas phase species to be simultaneously probed. We thereby observe that the Cu^{2+} oxidation state is stable in an atmosphere of O_2 (1 bar) but is spontaneously reduced under vacuum. We further show the detection of a range of gas phase species (CO, CO_2, O_2, Ar, N_2) in the pressure range 10-1500 mbar including species with low photoionization cross-sections (He and H_2). Pressure-dependent changes in the apparent binding energies of gas-phase species are observed that can be rationalized on the basis of changes in the work function of the metal-coated grids used to support the graphene membranes. We expect atmospheric pressure XPS based on this graphene membrane approach to be a valuable tool for the study of nanoparticle catalysis.

KEYWORDS: Graphene, Atmospheric Pressure, Photoelectron Spectroscopy, Nanoparticles, Catalysis

Determining the chemical state of a catalyst under realistic reaction conditions is of crucial importance in designing catalytic systems with improved activity and selectivity towards sought after products, and a key step in developing or improving existing industrial processes. X-ray photoelectron spectroscopy (XPS) has proved a powerful technique for providing quantitative and surface sensitive (within a few nm) information on the chemical composition of surfaces/interfaces. However, the ultra-high vacuum conditions needed for photoelectron detection in standard XPS systems significantly constrain the pressure range that can be explored, or else limits measurements to *post-mortem* examination following a higher-pressure reaction step. Attempts to perform measurements at higher pressures typically rely on a differentially pumped aperture placed between the sample and electron analyzer, which serves to increase the effective mean free-paths of the emitted photoelectrons.[1] The current generation of Ambient pressure (AP)XPS analyzers utilize electron optics to focus the photoelectrons through

several apertures as part of a multi-stage differentially pumped lens system, increasing the photoelectron collection efficiency and extending the measurement range up to tens of mbar.[2] These APXPS analyzers are now commercially available and installed in many lab-source and synchrotron-based systems around the world, and have been successfully applied to a broad range of research problems over the last decade.[3,4] Whilst this approach proves practical up to the tens of mbar regime, significant gas phase scattering of photoelectrons at higher pressures makes measurement impractical. However numerous reactions of interest occur at atmospheric pressures and above, and thus the behavior observed in existing APXPS systems may not be truly representative of such reactions.

To further bridge this "pressure gap" the differentially pumped aperture system may be replaced by a thin membrane, which promises a more abrupt change in pressure between the high-pressure cell and analyzer and thus a longer effective mean-free path for photoelectrons. Furthermore, it allows a uniform pressure to be maintained in the high-pressure cell, avoiding the inhomogeneous pressure distribution close to a differentially pumped aperture that constrains the minimum distance between sample and aperture.[4] The membrane must be strong enough to sustain the large pressure difference, yet thin enough to allow sufficient photoelectrons to pass through. Recent progress in the growth of uniform 2D materials over large-areas by chemical vapor deposition (CVD),[5–10] makes these materials promising candidates for achieving this. Graphene has been shown to be highly impermeable to gases and liquids,[11,12] while its thickness is below the inelastic mean free path (IMFP) lengths of the photoelectrons typically collected in XPS. Indeed, graphene layers have been used to maintain liquid environments under high vacuum conditions for electron microscopy measurements,[13–17] and to enable XPS of liquids where their transparency to photoelectrons was confirmed.[18] In addition, the good electrical conductivity of graphene means it can also serve as electrode/current collector for the study of electrochemical systems.[19]

Here we demonstrate single-layer graphene (SLG) membranes as supports for catalyst nanoparticles under atmospheric pressure reaction conditions (up to 1.5 bar) that are able to maintain pressure differences in excess of 6 orders of magnitude. Using these membranes we are able to detect a wide range of gases in the pressure range 10 mbar - 1500 mbar including N_2, Ar, CO_2, CO, and even He and H_2. We observe pressure-dependent changes in the gas-phase peak positions, which are rationalized on the basis of changes in the work function of the metal-coated grids used to support the graphene membranes. Our approach makes it possible to probe gas phase molecules as well as solid catalyst nanoparticles supported on the graphene film under reaction conditions.

Figure 1A shows a schematic cross-section of the reaction cell we use to perform atmospheric pressure XPS. A Polyether ether ketone (PEEK) enclosure is sealed with a graphene-based membrane sandwiched between a Viton® O-ring and stainless steel lid, which has a 2 mm aperture. Gas is supplied and removed from the cell by two PEEK tubes connected to holes in the rear of the cell and sealed using Apiezon® W wax. The graphene thereby separates the high-pressure gas environment within the reaction cell from the high vacuum conditions under which the analyzer is operated, whilst its thickness is below the IMFP of typical photoelectrons, allowing their escape to the vacuum side and collection by the analyzer (Figure 1B). Internal

pressures in excess of 1.5 bar can be sustained within the cell whilst the surrounding chamber is maintained well below 10^{-3} mbar.

The graphene-based membranes are produced by transferring CVD-grown SLG or bi-layer graphene (BLG) onto metal (Au or Al) coated silicon nitride grids using a polymer-free transfer technique (see Methods). Figure 1C shows a scanning electron microscopy (SEM) image of a region of the grids showing an array of 1 μm diameter holes with a uniform coverage of SLG. Careful inspection reveals linear features running from top left to bottom right, which are due to additional graphene layers formed near the rolling striations of the Cu foil substrate.[20] Figure 1D shows a scanning tunneling microscopy (STM) image of one of the SLG covered holes. The bulging region in the center corresponds to the suspended graphene. The region surrounding the hole shows nanoscale roughness from the evaporated Au film while STM images at high resolution revealed the honeycomb structure of the graphene. This, together with the lack of features related to surface contamination, confirms the cleanliness of our polymer-free transfer technique (see inset). Raman spectroscopy (Figure 1E) of the graphene transferred onto SiO_2(300 nm)/Si using the same polymer-free method shows the characteristic features of high-quality SLG, with a 2D peak well-fitted with a single Lorentzian function of 30 cm^{-1} fwhm, I_{2D}/I_G ratio of 2.27, and a negligible D peak.[21] This confirms that our transfer technique yields uniform graphene coverage over large areas, without inducing significant structural defects and avoiding the use of any supporting polymers, which otherwise leave residues that could reduce the photoelectron transmission of the membrane and be a source of contamination when studying reactions.[22]

Figures 2A shows the N 1s XP spectra measured using a Au-BLG membrane with the gas-cell filled with N_2 at pressures ranging from vacuum ($<10^{-3}$ mbar) up to 1 bar. Under vacuum a weak, broad peak is observed at 400 eV, which is assigned to N in the silicon nitride membrane. Similarly, Si peaks are also present in the survey spectra. Upon introduction of N_2, a sharp peak appears at ~405 eV that increases in intensity with pressure confirming it corresponds to the gas phase N_2. Whilst this peak increases in intensity with pressure, the silicon nitride related peak significantly weakens, as expected from its location ~30nm below the graphene layer (due to the metal layer between them) and the increased gas phase scattering of the photoelectrons. We thus confirm that our approach based on graphene membranes can readily detect gas phase species in the pressure range 10-1500 mbar.

Surprisingly the position of the gas phase peak is seen to shift to lower binding energies with increasing N_2 pressure, changing by ~0.7eV between 10 mbar and 1 bar. A similar behavior was observed for measurements of the Ar 2p core levels performed with Ar in the same pressure range. When similar measurements were instead performed with an Al-BLG membrane, no such shift in peak positions was observed (see Figure 2B).

The origin of the shift in gas phase peak positions seen for the Au membranes but not for the Al membranes becomes more apparent when considering the concomitantly measured C 1s XP spectra shown in Figure 2C and D. Under vacuum conditions the C 1s peak shape is broad, and is fitted by two main graphene components at ~284.4 eV (blue) and ~285.1 eV (purple) respectively.

The component at ~284.4 eV is consistent with the position of free-standing or weakly-coupled graphene,[23,24] and is thus predominantly attributed to graphene suspended over the holes in the membrane. A further contribution to this component is expected from the many small areas where the graphene does not fully conform to the nanoscale roughness of the Au interface (figure 1D). The peak at 285.1 eV is attributed to the regions of graphene in intimate contact with the Au surface where charge transfer leads to local doping of the graphene.[24–27]

When N_2(1 bar) is introduced behind the membrane the overall C 1s peak shape is found to be significantly narrower and shifted to lower binding energies (Figure 2C), indicating a reduction in the doped-graphene area (i.e., graphene in contact with Au). This could be due to intercalated N_2 gas that might increase the Au-graphene separation at the higher pressures, as seen with other gases for graphene on weakly interacting metals.[24,25,28–30] This is supported by the reversibility of the changes in the positions of the C 1s components with the addition/removal of the gas. The only exception to this is that the ongoing x-ray beam irradiation leads to some broadening of the C 1s peak on the high-binding energy side (grey component) which is attributable to defects induced in the graphene and/or the accumulation of defective carbon (as seen when comparing the C 1s peaks measured with 1 bar of N_2 which was collected ~1 hour before the measurement in vacuum).

For the Al-BLG membrane, no change in the position of the major C 1s component is observed with different gas pressures in the reaction cell, with only a broadening of the peak to higher binding energies observed with on-going beam exposure, related to the aforementioned formation of defects in the graphene and/or accumulation of carbonaceous species. This distinctively different behavior can be explained by considering that, in contrast to the Au, a stable oxide layer is formed on the surface of Al on air exposure. This insulating oxide layer electrically isolates the graphene from the metallic Al, preventing charge transfer from the Al to graphene and thus no doping related changes in C 1s peak are observed. Furthermore the oxide layer acts to passivate the Al surface, suppressing any significant changes in the Al work function under different gas environments, meaning the peak positions of gases in the reaction cell remain constant with pressure.

Further to the measurements of N_2 and Ar gases so far reported, we have also successfully detected O_2 (O 1s region), CO_2 and CO (both C 1s and O 1s regions – not shown). We next focus on the detection of gas phase species that are considered challenging to detect by XPS due to their low photoionization cross-sections. Figures 3 shows spectra obtained when the reaction cell is filled with Helium at different pressures. Although relatively weak, a distinct He 1s peak is clearly visible at ~19.9 eV binding energy (BE) relative to the analyzer Fermi level. Since the BE of He is 24.6 eV relative to the vacuum level,[31] it implies a work function of the Au-SLG membrane of 4.7 eV. The peak grows in intensity to give a strong, sharp peak as the He pressure is increased up to 1 bar. To achieve this, we use relatively low excitation energies (hν = 275 eV) to increase the He photoionization cross-section, and a SLG coated membrane to maximise the photoelectron transparency. We further test the threshold of gases we are able to detect by filling the reaction chamber with H_2 (1 bar). Here a distinct H 1s peak is observable at 11.2 eV (see Figure 3 inset), whose much lower intensity compared to the He 1s at He (1bar) is consistent with the ~30× lower photoionization cross-section of H_2 compared to He at similar photon energies.[32] The BE of the K level of H_2 being 15.4 eV[33] gives a work function of 4.2 eV for the

Au-SLG membrane, 0.5 eV smaller than with He, probably as a result of chemical changes in the Au-SLG membrane.

In addition to detecting the gas phase reactants/products, for *operando* catalytic studies we are also concerned with observing the chemical state of the catalyst itself under reaction conditions. To this end, we form Cu nanoparticles on the reaction chamber side of the graphene membrane by e-beam evaporation of Cu (1 nm nominal thickness). We note that these samples have been stored in laboratory air for several days prior to measurement. Figure 4A shows the structure of the as-deposited nanoparticles measured by scanning tunneling microscopy on a sample of freshly cleaved highly oriented pyrolytic graphitic (HOPG). The particles are ~10 nm in lateral dimension and 5-7 nm in height.

Figure 4B shows the evolution of the XP spectrum of our sample in the Cu 2p core level region as the environment within the gas cell is changed. Initially under vacuum the Cu 2p spectrum shows two sharp peaks at ~932 eV and ~955 eV, which can be assigned to the $2p_{1/2}$ and $2p_{3/2}$ core level peaks of Cu^0 metallic or Cu^{+1} oxidation states as these are difficult to distinguish by XPS alone.[34] Given the samples history of storage in air we attribute the oxidation state to the latter. On the introduction of the O_2 (1 bar) we observe distinct changes in the Cu 2p spectra with the broadening of these main peaks to higher binding energies and the appearance of features in the region between them which is characteristic of the Cu^{+2} oxidation state. The intensity loss and increased signal to noise ratio with the introduction of the oxygen indicates that the Cu XP signal not only originate from the surface of the Cu nanoparticles in contact with the graphene, but also from the nanoparticle surfaces in contact with the gas, where the photoelectrons must travel through the gas phase to reach the vacuum side of the membrane.

A second measurement some minutes later shows an increase in the proportion of Cu^{+2} indicating further oxidation of the Cu nanoparticles. On removing the O_2 and returning to vacuum, there is an immediate reduction of the Cu^{+2} demonstrating that the Cu^{+2} oxidation state is not stable under vacuum conditions, as also found by other authors[34,35] This highlights that the catalyst state can be greatly affected by changes in the pressure of reactants even in the absence of any heating, highlighting a key advantage of our atmospheric pressure XPS technique in reliably determining the state of the catalyst under reaction conditions.

To distinguish whether the increasing proportion of Cu^{+2} during measurement in O_2(1 bar) is due to the gradual oxidation of Cu with time, or if it is an effect of the high-intensity X-ray beam, we repeated the O_2 (1 bar) exposure but waited 15 min prior to collecting the first XP spectrum. The first spectrum appears similar to that previously taken without waiting for 15min indicating that the increase in the proportion of the Cu^{+2} oxidation state during measurement is induced, at least in part, by the X-ray beam presumably as a result of ionization of the high-pressure O_2.

Nevertheless we are clearly able to observe changes in the Cu nanoparticle oxidation state under atmospheric pressure reaction conditions. Figure 4C further shows the O 1s spectra measured with the gas cell under and vacuum ($<10^{-3}$ mbar) and filled with O_2 (1 bar), confirming that despite the graphene being covered with Cu nanoparticles the gas phase oxygen can also be

readily detected. This confirms the possibility of simultaneously measuring the catalyst state and gas phase reactants/products during an atmospheric pressure reaction.

In summary, we have shown that single-layer graphene membranes can maintain reaction cell pressures of at least 1.5 bar, whilst maintaining pressure differences in excess of 6 orders of magnitude. This allows the detection of various gases in the pressure range 10-1500 mbar using XPS. We show that the work function of the graphene support can influence the position of these gas phase peaks, depending on the gas environment within the reaction cell. These changes occur on Au supported graphene membranes but not on Al supported ones. We further show that gases with low photoionization cross-sections such as He and H_2 can be observed when present at pressures close to 1 bar. We have shown that the oxidation and reduction reactions of Cu nanoparticles deposited on the membranes under 1 bar of O_2 can be readily followed from the XPS signal obtained through the graphene. We expect that the graphene membrane approach shown here to be a valuable tool for future studies in catalysis.

METHODS

Cu foil coated with chemical vapor deposited (CVD) single layer graphene (SLG, Graphene Supermarket®) is first treated with an O_2-plasma to remove the SLG from one side. A supporting frame consisting of a ~10×10 mm^2 of adhesive Al foil with a centrally located ~8×8 mm^2 hole is then stuck to the untreated surface of a similarly sized piece of the SLG-Cu foil. The frame supported foil is then floated on the surface of a 50mL aqueous solution of ~0.1M $Na_2S_2O_8$ for ~4 hours to fully etch the Cu. The volume is then flushed with 2L of Milli-Q® water over the course of ~6 hours whilst maintaining the same volume of solution in the etching container and with the frame supported SLG remaining floating on top. To create BLG, another ~10×10 mm^2 of SLG-Cu foil is used to carefully lift the frame supported SLG out of water from below and left to dry. The etching and flushing processes are then repeated. Perforated TEM membranes (Pelco® Holey Silicon Nitride Support Films), each consisting of a 200 nm thick Si_3N_4 window with either a 40 × 40 array of Ø 1 μm circular holes at a 2 μm pitch or a 125 × 125 array of Ø 2 μm circular holes at a 4 μm pitch, are coated with either Al(30 nm) or Cr(3 nm)/Au(30 nm) conductive layer by thermal evaporation. These membranes are placed in the liquid below the frame supported SLG/BLG and lifted through it to capture the graphene and then left to dry for ~1hour. Successful SLG/BLG transfer is confirmed using scanning electron microscopy (SEM, Zeiss Supra55VP, 5 kV, in-lens detector). The deposition of Cu nanoparticles is achieved by e-beam evaporation of a nominally 1nm thick Cu layer onto the backside of the membranes.

In situ XPS measurements were performed using the APPES-II end station at beamline 11.0.2 of the Advanced Light Source, the Berkeley synchrotron facility. The setup consists of a vacuum chamber (base pressure ~10^{-6} mbar) attached to a set of three differentially pumped electrostatic lenses and a differentially pumped analyzer (Phoibos 150, SPECS GmbH), as described elsewhere.[36] All spectra are collected at an angle of 20° to normal emission, with a spot size of 60 × 200 μm^2. All binding energies are referenced to contemporaneously measured Fermi edges or the Au4f$_{7/2}$ peak which is fixed at 84.0eV. Gas pressures in the reaction cell are measured

using the mean value of two Granville Phillips 275 Convectron® gauges, one upstream and the other downstream of the reaction cell, with appropriate correction factors applied for the relevant gas species.

STM images were acquired using in a custom-built instrument using commercial Pt/Ir tips (Bruker PT10), with the tip grounded and the bias voltage (V_S) applied to the sample. Imaging parameters are indicated in the corresponding image captions.

AUTHOR INFORMATION

Corresponding Author

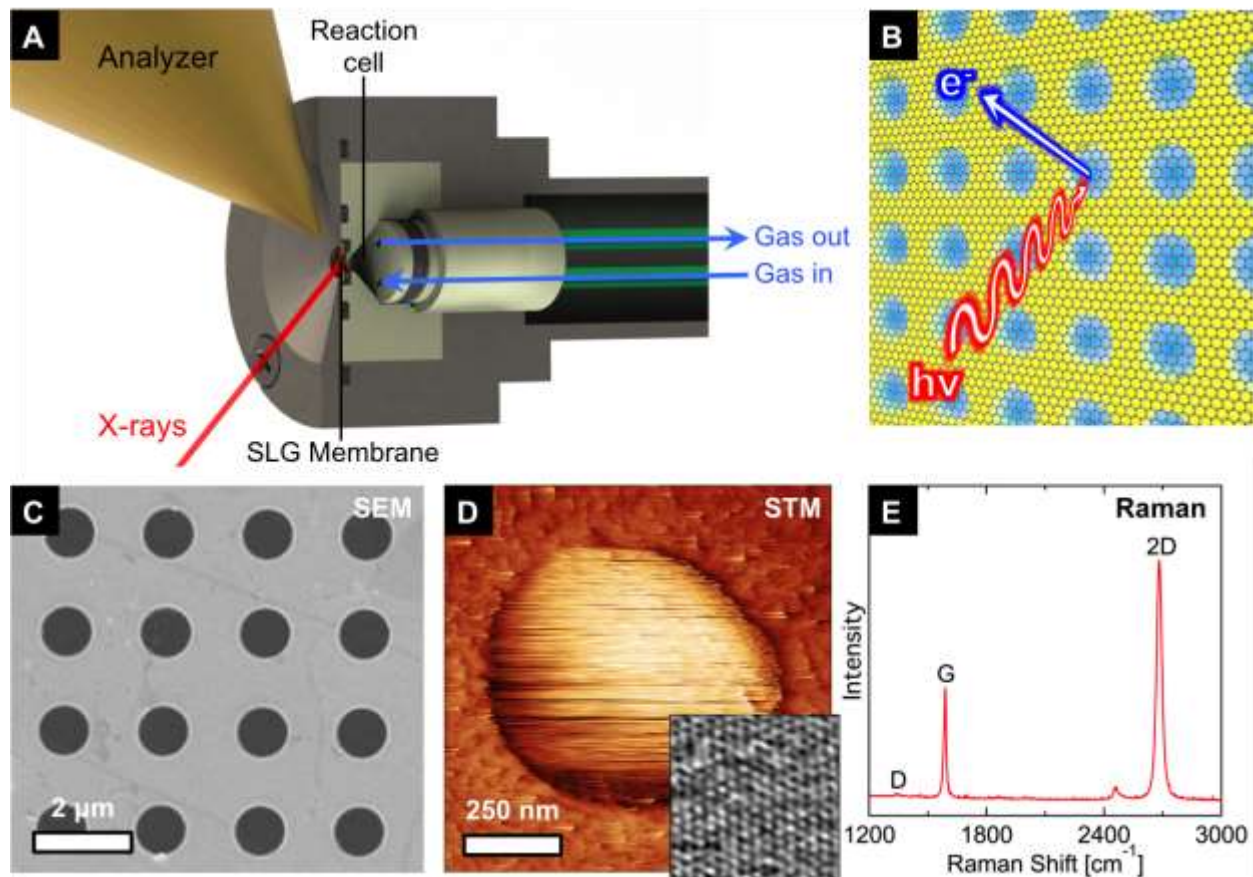*mbsalmeron@lbl.gov

FIGURES

Figure 1. (A) Cross-sectional view of the atmospheric pressure XPS setup showing the gas flow through the reaction cells and the approximate arrangement of the analyser and X-ray beam. (B) Sketch of the graphene-based membrane illustrating the operating principal of atmospheric pressure XPS. (C) SEM image of a region of a SLG covered membrane. D) STM image of one the holes in the membrane with SLG suspended across it (V_S= 1.5 V, I_t= 300 pA). Inset: Atomic resolution STM image of free-standing graphene measured in the hole region (V_S= 0.18 V, I_t= 500 pA, 2D-FFT filtered). E) Representative Raman spectra of SLG transferred onto SiO_2(300 nm)/Si using the same polymer-free method used for fabricating the graphene-based membranes.
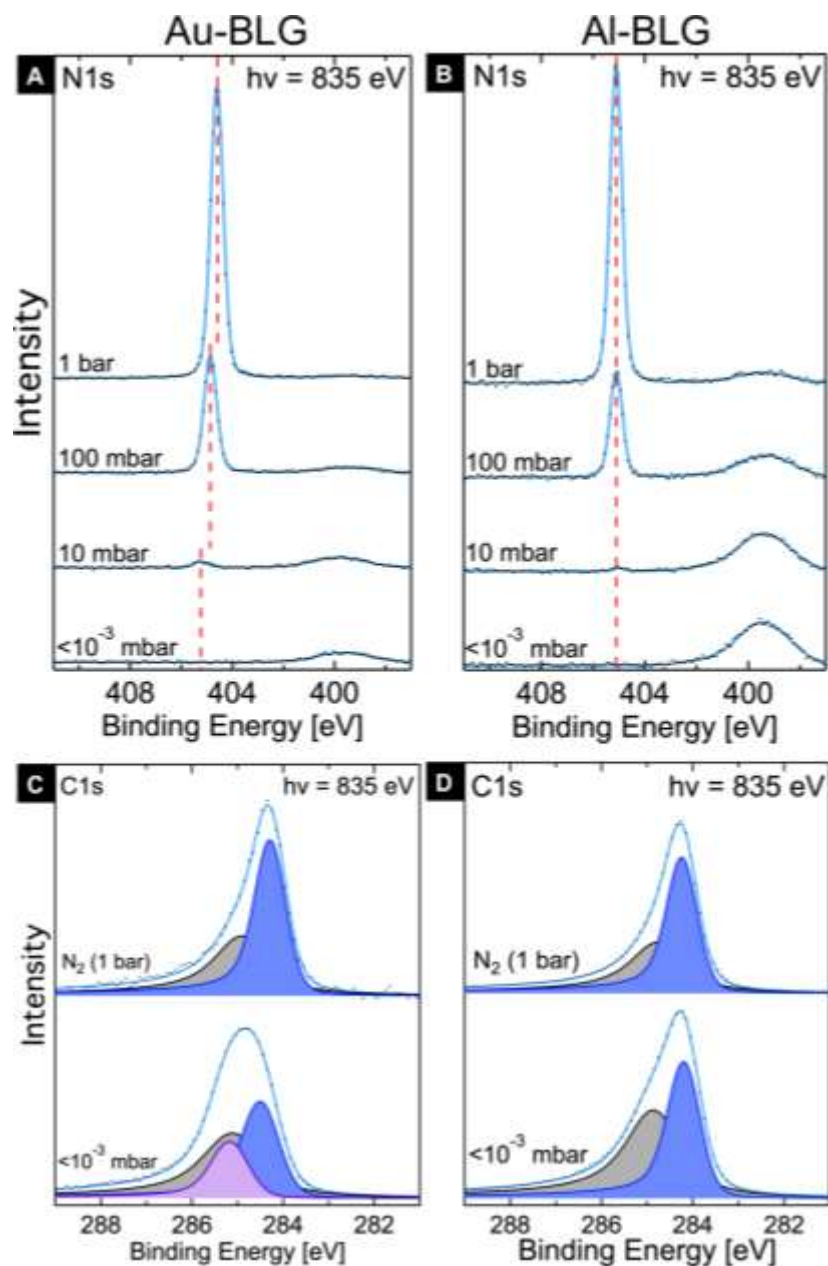
Figure 2. A,B) N 1s XP spectra collected using a Au-BLG (A) or Al-BLG (B) membrane with the reaction cell under vacuum (<10^{-3} mbar), and filled with N$_2$ (10mbar, 100 mbar, and 1 bar). C,D) Corresponding C 1s spectra collected using a Au-BLG (C) or Al-BLG (D) membrane with the reaction cell under vacuum (<10^{-3} mbar), and filled with N$_2$ (1 bar). The spectra are collected with photon energies, hv = 835 eV, and are background corrected (Shirley for silicon nitride and C 1s peaks, linear for N$_2$ peaks) and analyzed by performing a non-linear mean square fit of the data, using Doniach-Šunjić functions convoluted with Gaussian profiles.
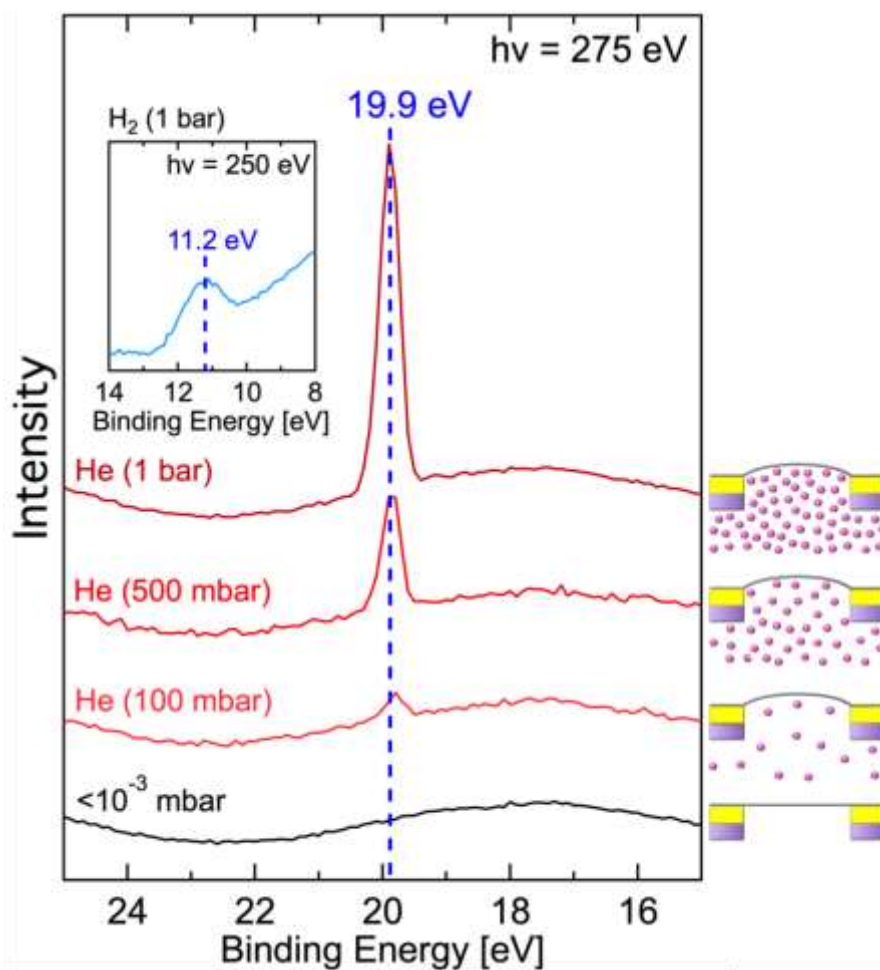
Figure 3. He 1s XP spectra collected using a Au-SLG membrane with the reaction cell under vacuum ($<10^{-3}$ mbar), and filled with He (100 mbar, 500 mbar, and 1 bar) with photon energies of hν = 275 eV. Inset: H 1s spectra measured with the same membrane, with the reaction cell filled with H_2 (1 bar) and photon energy, hν = 250 eV. No background correction is performed.
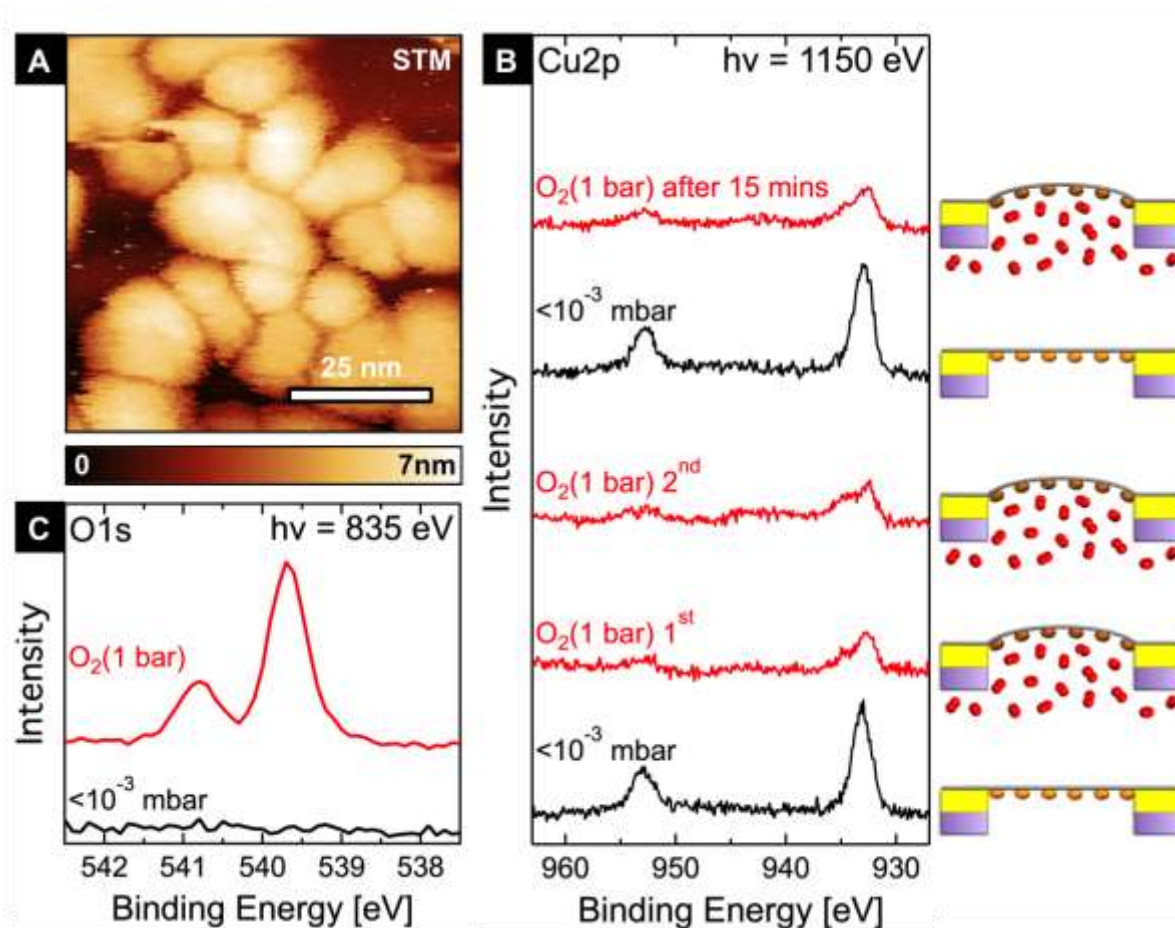
Figure 4. A) STM image of Cu nanoparticles formed by e-beam evaporation of Cu (1 nm nominal thickness) onto HOPG (V_S= 2.5 V, I_t= 40 pA). B) Cu2p XP spectra for an Au-SLG membrane covered with Cu(1 nm) measured under vacuum ($<10^{-3}$ mbar), 1st and 2nd spectra measured in presence of O_2 (1 bar), measured again under vacuum ($<10^{-3}$ mbar), and measured after 15 min of O_2 (1 bar) exposure with the X-ray beam blanked. The spectra are collected with a photon energy. hν = 1150 eV. C) The corresponding O 1s XP spectra measured under vacuum ($<10^{-3}$ mbar) and in the presence of O_2 (1 bar) using photon energies, hν = 835 eV. All spectra are background corrected (Shirley for Cu peaks, linear for gas-phase O_2 peaks)

REFERENCES

(1)   Siegbahn, K.; Nordling, C.; Johansson, G.; Hedman, J.; Hedén, P. F.; Hamrin, K.; Gelius, U.; Bergmark, T.; Werme, L. O.; Manne, R.; et al. *ESCA Applied to Free Molecules*; North-Holland Publishing Company: Amsterdam-London, 1969.

(2)   Ogletree, D. F.; Bluhm, H.; Lebedev, G.; Fadley, C. S.; Hussain, Z.; Salmeron, M. A Differentially Pumped Electrostatic Lens System for Photoemission Studies in the Millibar Range. *Rev. Sci. Instrum.* **2002**, *73* (11), 3872.

(3)   Bluhm, H. Preface to the Special Issue of Topics in Catalysis on Ambient Pressure X-Ray Photoelectron Spectroscopy. *Top. Catal.* **2016**, *59* (5-7), 403–404.

(4)   Starr, D. E.; Liu, Z.; Hävecker, M.; Knop-Gericke, A.; Bluhm, H. Investigation of Solid/vapor Interfaces Using Ambient Pressure X-Ray Photoelectron Spectroscopy. *Chem. Soc. Rev.* **2013**, *42* (13), 5833–5857.

(5)   Li, X.; Cai, W.; An, J.; Kim, S.; Nah, J.; Yang, D.; Piner, R.; Velamakanni, A.; Jung, I.; Tutuc, E.; et al. Large-Area Synthesis of High-Quality and Uniform Graphene Films on Copper Foils. *Science* **2009**, *324* (5932), 1312–1314.

(6)   Weatherup, R. S.; Dlubak, B.; Hofmann, S. Kinetic Control of Catalytic CVD for High Quality Graphene at Low Temperatures. *ACS Nano* **2012**, *6* (11), 9996–10003.

(7)   Hofmann, S.; Braeuninger-Weimer, P.; Weatherup, R. S. CVD-Enabled Graphene Manufacture and Technology. *J. Phys. Chem. Lett.* **2015**, *6*, 2714–2721.

(8)   Caneva, S.; Weatherup, R. S.; Bayer, B.; Brennan, B.; Spencer, S. J.; Mingard, K.; Cabrero-Vilatela, A.; Baehtz, C.; Pollard, A. J.; Hofmann, S. Nucleation Control for Large, Single Crystalline Domains of Monolayer Hexagonal Boron Nitride via Si-Doped Fe Catalysts. *Nano Lett.* **2015**, *15*, 1867–1875.

(9)   Caneva, S.; Weatherup, R. S.; Bayer, B. C.; Blume, R.; Cabrero-Vilatela, A.; Braeuninger-Weimer, P.; Martin, M.-B.; Wang, R.; Baehtz, C.; Schlögl, R.; et al. Controlling Catalyst Bulk Reservoir Effects for Monolayer Hexagonal Boron Nitride CVD. *Nano Lett.* **2016**, *16*, 1250–1261.

(10)   Cabrero-Vilatela, A.; Weatherup, R. S.; Braeuninger-Weimer, P.; Caneva, S.; Hofmann, S. Towards a General Growth Model for Graphene CVD on Transition Metal Catalysts. *Nanoscale* **2015**, *8*, 2149–2158.

(11)   Bunch, J. S.; Verbridge, S. S.; Alden, J. S.; van der Zande, A. M.; Parpia, J. M.; Craighead, H. G.; McEuen, P. L. Impermeable Atomic Membranes from Graphene Sheets. *Nano Lett.* **2008**, *8* (8), 2458–2462.

(12)   Walker, M. I.; Weatherup, R. S.; Bell, N. A. W.; Hofmann, S.; Keyser, U. F. Free-Standing Graphene Membranes on Glass Nanopores for Ionic Current Measurements. *Appl. Phys. Lett.* **2015**, *106*, 023119.

(13)   Krueger, M.; Berg, S.; Stone, D.; Strelcov, E.; Dikin, D. A.; Kim, J.; Cote, L. J.; Huang, J.; Kolmakov, A. Drop-Casted Self-Assembling Graphene Oxide Membranes for Scanning Electron Microscopy on Wet and Dense Gaseous Samples. *ACS Nano* **2011**, No. 12, 10047–10054.

(14)   Yuk, J. M.; Park, J.; Ercius, P.; Kim, K.; Hellebusch, D. J.; Crommie, M. F.; Lee, J. Y.; Zettl, A.; Alivisatos, A. P. High-Resolution EM of Colloidal Nanocrystal Growth Using Graphene Liquid Cells. *Science* **2012**, *336* (6077), 61–64.

(15) Wang, C.; Qiao, Q.; Shokuhfar, T.; Klie, R. F. High-Resolution Electron Microscopy and Spectroscopy of Ferritin in Biocompatible Graphene Liquid Cells and Graphene Sandwiches. *Adv. Mater.* **2014**, *26* (21), 3410–3414.

(16) Park, J.; Elmlund, H.; Ercius, P.; Yuk, J. M.; Limmer, D. T.; Chen, Q.; Kim, K.; Han, S. H.; Weitz, D. A.; Zettl, A.; et al. 3D Structure of Individual Nanocrystals in Solution by Electron Microscopy. *Science* **2015**, *349* (6245), 290–295.

(17) Park, J.; Park, H.; Ercius, P.; Pegoraro, A. F.; Xu, C.; Kim, J. W.; Han, S. H.; Weitz, D. A. Direct Observation of Wet Biological Samples by Graphene Liquid Cell Transmission Electron Microscopy. *Nano Lett.* **2015**, *15* (7), 4737–4744.

(18) Kolmakov, A.; Dikin, D. a; Cote, L. J.; Huang, J.; Abyaneh, M. K.; Amati, M.; Gregoratti, L.; Günther, S.; Kiskinova, M. Graphene Oxide Windows for in Situ Environmental Cell Photoelectron Spectroscopy. *Nat. Nanotechnol.* **2011**, *6* (10), 651–657.

(19) Velasco-Velez, J. J.; Pfeifer, V.; Hävecker, M.; Weatherup, R. S.; Arrigo, R.; Chuang, C.-H.; Stotz, E.; Weinberg, G.; Salmeron, M.; Schlögl, R.; et al. Photoelectron Spectroscopy at the Graphene-Liquid Interface Reveals the Electronic Structure of an Electrodeposited Cobalt/Graphene Electrocatalyst. *Angew. Chemie Int. Ed.* **2015**, n/a – n/a.

(20) Kidambi, P. R.; Ducati, C.; Dlubak, B.; Gardiner, D.; Weatherup, R. S.; Martin, M.-B.; Seneor, P.; Coles, H.; Hofmann, S. The Parameter Space of Graphene Chemical Vapor Deposition on Polycrystalline Cu. *J. Phys. Chem. C* **2012**, *116* (42), 22492–22501.

(21) Ferrari, A.; Meyer, J.; Scardaci, V.; Casiraghi, C.; Lazzeri, M.; Mauri, F.; Piscanec, S.; Jiang, D.; Novoselov, K.; Roth, S.; et al. Raman Spectrum of Graphene and Graphene Layers. *Phys. Rev. Lett.* **2006**, *97*, 187401.

(22) Kratzer, M.; Bayer, B. C.; Kidambi, P. R.; Matković, A.; Gajić, R.; Cabrero-, A.; Weatherup, R. S.; Hofmann, S.; Teichert, C. Effects of Polymethylmethacrylate-Transfer Residues on the Growth of Organic Semiconductor Molecules on Chemical Vapor Deposited Graphene. *Appl. Phys. Lett.* **2015**, *106*, 103101.

(23) Weatherup, R. S.; Amara, H.; Blume, R.; Dlubak, B.; Bayer, B. C.; Diarra, M.; Bahri, M.; Cabrero-vilatela, A.; Caneva, S.; Kidambi, P. R.; et al. Interdependency of Subsurface Carbon Distribution and Graphene-Catalyst Interactions. *J. Am. Chem. Soc.* **2014**, *136*, 13698–13708.

(24) Weatherup, R. S.; D'Arsié, L.; Cabrero-Vilatela, A.; Caneva, S.; Blume, R.; Robertson, J.; Schlögl, R.; Hofmann, S. Long-Term Passivation of Strongly Interacting Metals with Single-Layer Graphene. *J. Am. Chem. Soc.* **2015**, *137*, 14358–14366.

(25) Blume, R.; Kidambi, P. R.; Bayer, B. C.; Weatherup, R. S.; Wang, Z.-J.; Weinberg, G.; Willinger, M.-G.; Greiner, M.; Hofmann, S.; Knop-Gericke, A.; et al. The Influence of Intercalated Oxygen on the Properties of Graphene on Polycrystalline Cu under Various Environmental Conditions. *Phys. Chem. Chem. Phys.* **2014**, *16*, 25989–26003.

(26) Dahal, A.; Batzill, M. Graphene-Nickel Interfaces: A Review. *Nanoscale* **2014**, *6* (5), 2548–2562.

(27) Voloshina, E.; Dedkov, Y. Graphene on Metallic Surfaces: Problems and Perspectives. *Phys. Chem. Chem. Phys.* **2012**, *14* (39), 13502–13514.

(28) Larciprete, R.; Ulstrup, S.; Lacovig, P.; Dalmiglio, M.; Bianchi, M.; Mazzola, F.; Hornekær, L.; Orlando, F.; Baraldi, A.; Hofmann, P.; et al. Oxygen Switching of the Epitaxial Graphene-Metal Interaction. *ACS Nano* **2012**, *6* (11), 9551–9558.

(29) Grånäs, E.; Andersen, M.; Arman, M. a.; Gerber, T.; Hammer, B.; Schnadt, J.; Andersen, J. N.; Michely, T.; Knudsen, J. CO Intercalation of Graphene on Ir(111) in the Millibar Regime. *J. Phys. Chem. C* **2013**, *117* (32), 16438–16447.

(30) Grånäs, E.; Knudsen, J.; Schröder, U. a; Gerber, T.; Busse, C.; Arman, M. a; Schulte, K.; Andersen, J. N.; Michely, T. Oxygen Intercalation under Graphene on Ir(111): Energetics, Kinetics and the Role of Graphene Edges. *ACS Nano* **2012**, *6* (11), 9951–9963.

(31) Bearden, J. A.; Burr, A. F. Reevaluation of X-Ray Atomic Energy Levels. *Rev. Mod. Phys.* **1967**, *39* (1), 125–142.

(32) Yeh, J. J.; Lindau, I. Atomic Subshell Photoionization Cross Sections and Asymmetry Parameters: $1 \leq Z \leq 103$. *At. Data Nucl. Data Tables* **1985**, *32* (1), 1–55.

(33) Herzberg, G. Dissociation Energy and Ionization Potential of Molecular Hydrogen. *Phys. Rev. Lett.* **1969**, *23* (19), 1081–1083.

(34) Jiang, P.; Prendergast, D.; Borondics, F.; Porsgaard, S.; Giovanetti, L.; Pach, E.; Newberg, J.; Bluhm, H.; Besenbacher, F.; Salmeron, M. Experimental and Theoretical Investigation of the Electronic Structure of Cu2O and CuO Thin Films on Cu(110) Using X-Ray Photoelectron and Absorption Spectroscopy. *J. Chem. Phys.* **2013**, *138* (2), 024704–1 – 024704–024706.

(35) Lee, S. Y.; Mettlach, N.; Nguyen, N.; Sun, Y. M.; White, J. M. Copper Oxide Reduction through Vacuum Annealing. *Appl. Surf. Sci.* **2003**, *206* (1-4), 102–109.

(36) Bluhm, H.; Hävecker, M.; Knop-Gericke, A.; Kiskinova, M.; Schlögl, R.; Salmeron, M. In Situ X-Ray Photoelectron Studies of Gas - Solid Interfaces at Near- Ambient Conditions. *MRS Bull.* **2007**, *32* (December), 1022–1030.